Experiments in Fluids 28 (2000) 74–85 © Springer-Verlag 2000

Drag reduction of motor vehicles by active flow control using the Coanda effect

D. Geropp, H.-J. Odenthal

Abstract A test facility has been constructed to realistically simulate the flow around a two dimensional car shaped body in a wind tunnel. A moving belt simulator has been employed to generate the relative motion between model and ground. In a first step, the aerodynamic coefficients c_L and c_D of the model are determined using static pressure and force measurements. LDA-measurements behind the model show the large vortex and turbulence structures of the near and far wake. In a second step, the ambient flow around the model is modified by way of an active flow control which uses the Coanda effect, whereby the base-pressure increases by nearly 50% and the total drag can be reduced by 10%. The recirculating region is completely eliminated. The current work reveals the fundamental physical phenomena of the new method by observing the pressure forces on the model surface as well as the time averaged velocities and turbulence distributions for the near and far wake. A theory resting on this empirical information is developed and provides information about the effectiveness of the blowing method. For this, momentum and energy equations were applied to the flow around the vehicle to enable a validation of the theoretical results using experimental values.

List of symbols

A_F	surface of the suction slots (4.95×10^{-3} m^2)
A_R	surface of blowing slots (1.66×10^{-3} m^2)
B	model width (0.665 m)
c_D	drag coefficient
c_{DP}	pressure drag coefficient
$c_{DP,B}$	base-pressure drag coefficient
c_f	skin-friction coefficient
c_L	lift coefficient
c_{LP}	pressure lift coefficient
$c_{LP,B}$	base-pressure lift coefficient
c_P	pressure coefficient
F	force
F_S	supporting force
g	acceleration due to gravity
h	clearance between model and ground (20.5 mm)
H	model height (0.147 m)
h_B	model base height between blowing slots (0.112 m)
I	momentum
k	turbulence energy
L	model length (0.506 m)
$\dot{m}$	mass flow rate
p	pressure
P	aerodynamic engine power
P_C	compressor power
Re	Re-number, based on model length
t	time
u,v,w	velocities in x,y,z-direction
u',v',w'	fluctuating velocities
x,y,z	coordinates
$\dot{V}$	volume flow rate
Δp_C	increase of pressure of the compressor

Greek symbols

α	angle of rear blowing slot
λ	laser wavelength
ρ	density of air
Ψ	stream function
τ	shear stress
η_C	loss factor of compressor
ζ_R	blowing rate

Subscripts

a	without flow control
B	base
b	with flow control
D	drag
F	front
L	lift
P	pump
R	rear
t	tangential
∞	freestream condition

Received: 9 June 1998 / Accepted: 20 July 1999

D. Geropp, H.-J. Odenthal[1]
Institut für Fluid- und Thermodynamik
Universität-GH Siegen
Paul-Bonatz-sb. 9–11, D-57076 Siegen, Germany

[1]*Present address*:
Institut für Industrieofenbau und
Wärmetechnik, RWTH Aachen
Kopernikusstr. 16, D-52074 Aachen, Germany

Correspondence to: D. Geropp

This paper is dedicated to Prof. Dr. sc. tech. J.U. Keller on the occasion of his 60th birthday.

The authors would like to acknowledge the very generous support and keen interest of Daimler-Chrysler AG, Stuttgart.

1
Introduction

Essentially, the road resistance of a motor vehicle consists of a mechanical and an aerodynamic part. At high speeds the aerodynamic component dominates, whereby the aerodynamic pressure drag is predominant. As is the case with all bluff bodies, the pressure drag is due to separation effects which induce intensive turbulent vortex structures with high dissipation.

Although numerical methods as the Navier-Stokes solvers (Han et al. 1996; Ramnefors et al. 1996) or the so called multi-zone methods (e.g. Geropp and Kim 1995; Geropp and Mildebrath 1995) have made considerable progress recently, the used turbulence models, especially for the near wake, also called dead water, show partly large deficits at calculating details in the flow field. Thus, the base pressure and the aerodynamic forces can not be exactly enough determined.

Another aspect, often neglected in theory and experiment, is the influence of the ground effect (car/road) on the flow field and especially on the dead water. In this case a loss of accuracy of the aerodynamic coefficients can be observed as references (Bearman et al. 1988; Hucho 1994; Kronast 1992; Odenthal 1997; Wiedemann 1989) confirm.

In addition, for the drag reduction of bluff bodies it is very important to change the turbulent vortex structures in the dead water, the region with the highest dissipation processes. But therefore the physical details of the universal principles of the dissipation region must be known. With respect to these details, this paper makes a first basic contribution. Furthermore, for the validation and improvement of applied turbulence models as well as for the drag reduction intensive measurements of local time averaged velocities, pressure distributions and Reynolds stresses must be realized. The often applied recording of the integral forces as lift and drag is not sufficient enough to detect detailed flow phenomena.

Now, if one considers the separation at the rear side of a bluff body, two fundamental cases can be distinguished (e.g. Hucho 1994): If the edges of the body are vertical to the main flow, then vortices with axes parallel to the separation lines will develop. The shear layers behind the body interact to form a recirculating region and two contra-rotating time averaged stationary vortices appear. This typical form of the dead water for all two-dimensional bluff bodies also extends across the three-dimensional rear of a motor vehicle. As a consequence the region is generally perceived as being two-dimensional.

On the contrary, if the separation occurs at diagonal edges, induced vortices will be developed in form of opposite vortex pairs similar to wing-tip vortices. Their axes adjust in the longitudinal direction of the body. At a motor vehicle, such vortex pairs are observed mainly on the passages to the rear window, the so called C-column. They superpose the mentioned cross vortices and change the pressure drag. Because the cross vortices dominate the dead water, especially in the case of bluff bodies, the demonstrated experimental investigations were restricted to a two-dimensional car model with vertical rear side.

To reduce the drag, the pressure drag and more specifically the structure of the dead water must be changed as above mentioned. Passive processes can be used to control the flow such as attaching long splitter-plates to the rear side as shown by Apelt et al. (1973), Leder (1992), Soja (1994) or by realizing boat-tailing. These measures are however exhausted for stylistic and safety-related reasons, which underline the need for more active processes such as modifying the dead water using suction and/or blowing (Freund et al. 1994; Geropp 1991, 1995; Gersten and Wiedemann 1982; Odenthal 1997; Soja 1994).

References from Geropp (1991, 1995) describe a method to influence the rear region of vehicles, e.g. road or rail vehicles. The method intends to modify the two-dimensional vortex pair which is generated by the underbody and top flow of a car by tangentially blowing into the base dead water using the Coanda effect. It is known that the Coanda effect describes the behavior of a free jet which adheres to a curved surface and then follows the contour of the surface (Truckenbrodt 1980). Comprehensive investigations to the Coanda effect have been carried out by Fernholz (1966). Likewise, it is possible to influence the mentioned longitudinal vortices behind a three-dimensional car model as shown by Eberz (1997) at the Institute of Fluid- and Thermodynamics, Siegen.

To influence the two-dimensional dead water behind a car model, air is taken from the ambient flow at such positions of the surface, where high-pressure exists (e.g. the front of the car). The air is accelerated by a blower into the car and again is blown out over two horizontal slots in the area of the upper and lower separation lines (see Fig. 1). Both jets stay attached on the base surface due to the Coanda effect and cause a rise in pressure in the area of the stagnation streamline. The outer flow is entrained by Coanda blowing, the separation is prevented and the dead water gets new energy. Simultaneously the normal wake structure is changed considerably. The combination of tangential blowing into the dead water, diversion of jets and outer flow by the Coanda

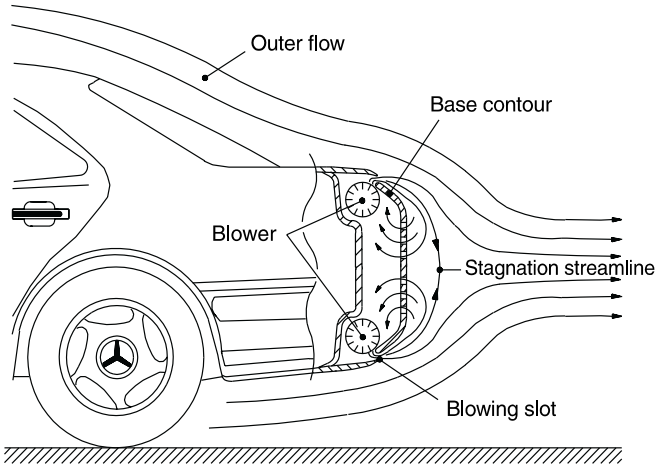

Fig. 1. Sketch showing the method of active flow control according to Geropp (1991, 1995)

effect leads to a reduction in dissipation, an increasing base-pressure and consequently a reduction of the total drag. The main intention of this study is it to reveal the physical mechanism of the new method by means of investigations into a two-dimensional motor vehicle through pressure, force and LDA-measurements.

2 Facility and measurement technique

The experiments were carried out in an 80 kW-Göttingen type wind tunnel with an open test section length of 2.4 m and a nozzle dimension of 1 m × 1 m. The contraction ratio of the nozzle is 6.8. In this work, the maximum freestream velocity is $u_\infty = 30$ m/s. This value corresponds to Re = 9.9×10^5, based on the model length L. The turbulence intensity in the empty test section is less than 1%.

To simulate the relative motion between vehicle and road, a moving belt simulator is used (see Fig. 2). It essentially consists of two components, the moving belt and the boundary layer suction facility. The smooth belt runs over two cylinders, of which only one is driven. The belt length in the test section totals 1.73 m and the width 1.01 m. The large belt length is important as it is necessary to simulate the interactions between the moving ground and the wake correctly as references from Bearman et al. (1988), Kronast (1992), Odenthal (1997) show. The driving unit has a power output of 20 kW. The belt speed, which is always the same as the speed in the tunnel, can be controlled to 0.5% exactly. The cylinders run on bearings in a large frame, which is vertically adjustable. To receive homogeneous velocity distributions, the nozzle boundary layer is separated by a 30 mm high gap between the lower surface of the nozzle and the simulator. The front plate of the simulator (l = 330 mm) is shaped elliptically to get a non-separated flow. The new boundary layer, which is generated at the plate, is sucked over a perforation with a double-flow periphery pump of 11 kW. Behind the section of the boundary layer suction, a steel sheet is attached to ensure a smooth motion between the fixed plate and the moving belt. Measurements from Odenthal (1997) above the belt with a Constant-Temperature-Anemometer (CTA) have shown that homogeneous velocity distributions develop up to $u_\infty = 40$ m/s. The system of coordinates is also defined in Fig. 2.

The investigations were carried out on a 1/5-scale, two-dimensional car model (see Fig. 3). The reason for choosing a two-dimensional model was to reveal and to understand the physical details of the new Coanda blowing method in conjunction with the ground effect. The total length of the model is L = 0.506 m, height H = 0.147 m and width B = 0.665 m (B/H = 4.52). The base height is h_B = 0.112 m. To get a base-pressure as high as possible, the model has an underbody diffuser with a deflection angle of 5°. The clearance h between the ground surface and the underbody of the model is 20.5 mm being typical for real motor vehicles.

In order to guarantee a two-dimensional flow the model is restricted by two plexiglass end plates (1.5 m × 1.0 m × 0.008 m) on both ends which are suspended vertically in the test section. To make sure that reaction forces are not transmitted to the balance, the plates do not touch the model that means there is small gap of 1.5 mm between the plates and the model. This ensures that the side flow around the model due to the pressure differences is avoided. The end plates are elliptically shaped and are limited below by brushes against the moving belt. They project the model over the 1.5 fold model length to enable non-interference wake measurements and to provide a nearly two-dimensional wake.

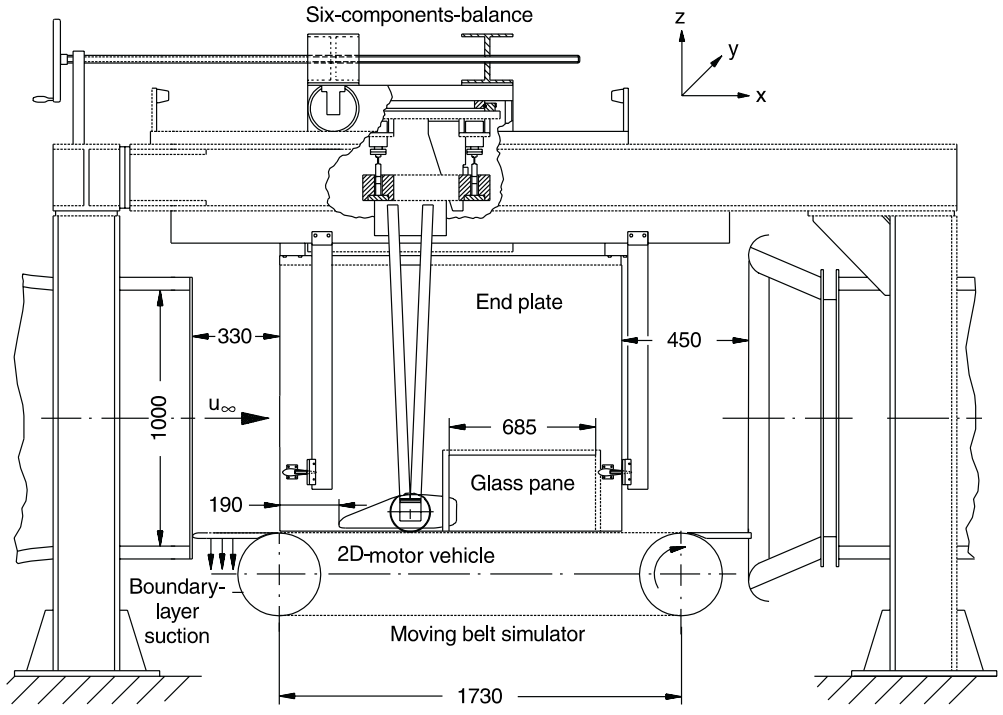

Fig. 2. Side view of the wind tunnel test section with two-dimensional motor vehicle model

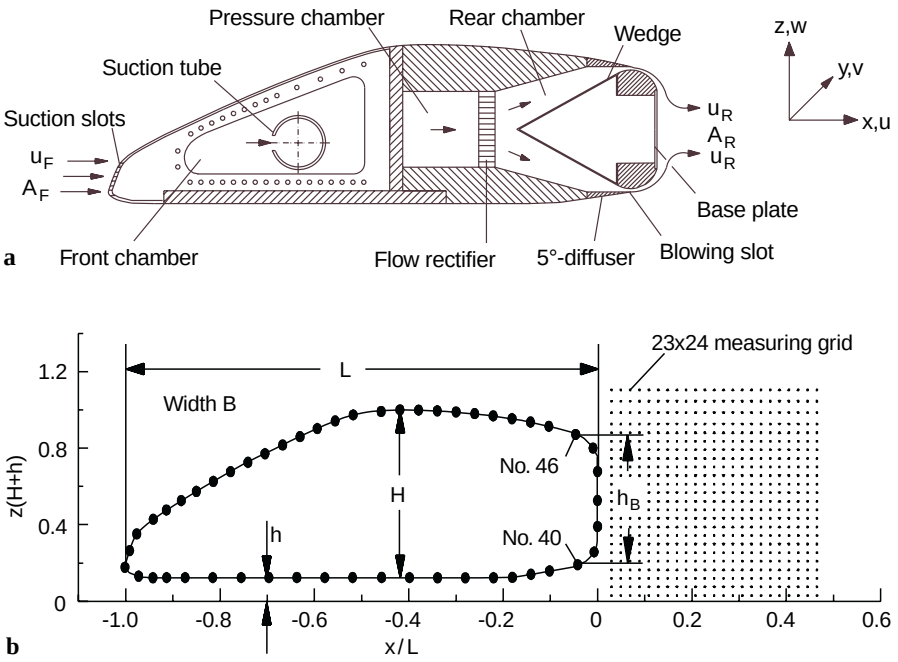

Fig. 3. a Construction of the two-dimensional car model. **b** Arrangement of pressure taps and LDA-measuring grid in the middle span

To influence the flow, two independent pressure chambers are positioned within the car model (Fig. 3a). Five slot lines in the front of the car with a total area of $A_F = 4.95 \times 10^{-3}$ m^2 are used to take air from the main flow. The volume flow rate is marked with $\dot{V}_F$ and the averaged suction velocity with u_F. The volume flow rate determined with a specifically developed measuring technique, which does not influence the balance measurements, is described in detail by Odenthal (1997). The suction out of the internal front chamber is realized by a PVC-tube with a longitudinal slot which is variable in y-direction. The volumetric flow is then conducted to the inlet side of a second external periphery pump of the same type as the first one. This pump delivers the air across a flow rectifier into the rear chamber where it is divided into the upper and lower slot and then blown out into the dead water with the blowing velocity u_R. All experiments were conducted with identical volumetric flows at the front and rear side ($\dot{V}_F = \dot{V}_R$). The blowing or jet flow rate

$$\zeta_R = \frac{u_R}{u_\infty} \quad , \qquad (1)$$

defined as the ratio of blowing to freestream velocity was only varied by changing the main speed u_∞. In this study the blowing rate varied from two to six.

The investigations of the aerodynamic behavior of the model were carried out using three different measurement techniques: To measure the pressure distributions, 57 static-pressure taps, each with a diameter of 0.8 mm, were distributed at the surface of the model, from which 51 can be found in the center of the span ($y/B = 0$). To examine the two-dimensionality of the flow, there are 6 further taps outside the middle at the position $y/B = \pm 0.2$. Using a scanivalve-system and two pressure gauges, the model pressures could be measured and so the pressure lift coefficient c_{LP} and the pressure drag coefficient c_{DP} can be determined as well. They are marked as taps No. 40 and 46 in Fig. 3b and are found directly in the lower and upper blowing slot. The surface between both slots (base height: h_B = 0.112 m) is responsible for the development of the base-pressure drag coefficient $c_{DP,B}$.

In comparison to the pressure measurements, the six-components-balance registers both the frictional and the pressure forces so that the total lift and drag coefficients c_L and c_D can also be determined.

In most cases the integral pressure and force measurement with pressure gauge and balance prevents the resolution of individual flow phenomena like flow separation. More detailed information can be obtained by measuring the time averaged velocities and turbulence intensities around the car with the high-resolution LDA-technique.

The velocities in the dead water and near wake were measured with a 3-beam two-component laser Doppler anemometer (LDA) working in backscattering mode. A 5 W-Argon-ion-laser is used whose blue-green beam is divided into two partial beams with identical light power. One beam is divided by a beamsplitter into a blue ($\lambda_{bl} = 488.0$ nm) and a green ($\lambda_{gr} = 514.5$ nm) component. Both beams, which were shifted by a Bragg cell of 40 MHz, as well as the non-shifted blue-green beam are directed over two 45°-mirrors to the front lens. The measuring volume has a diameter of about 0.16 mm and a length of 5.5 mm, the fringe space totals 8.5 μm. The front lens and both 45°-mirrors are part of a three-dimensional traversing system which can be addressed by an IEEE-interface card.

The backscattered light out of the measuring volume passes the front lens, the mirrors, a pinhole which serves as a spatial filter and enters the backscatter receiver optics. Subsequently, two photomultipliers transform the optic into electrical signals. Since the transmitter optics is also receiver optics, the time-consuming adjustment of the photomultipliers is avoided when the measuring grid

point changes. The electrical signals were shifted, amplified, bandpassfiltered and processed by counter-processors. The validity of the measurements is examined through a 5/8-comparison. The coincidence time totals 10 ms and measuring errors due to biasing can be minimized using a residence time weighting. A water-glycerin mix (10:1) seeds the flow. The particles have a diameter of 0.8 μm to 1.5 μm and so they are small enough to track the flow accurately and large enough to scatter light.

3 Experimental results

Initially, the influence of a stationary and moving ground on the aerodynamic coefficients should be clarified before realizing the new blowing method. Figure 4 shows c_P-pressure distributions on the model contour exemplary at Re = 9.9×10^5, stationary and moving ground and a typical ground clearance of $h/L = 0.04$.

At the front stagnation point the flow is divided in an upperbody and underbody model flow. The upper one accelerates up to the position of the maximum model height at $x/L = -0.5$ and subsequently decelerates to the constant base-pressure of $c_P = -0.334$. All investigations indicate that variable Re-numbers do not change the pressure at the upper side of the model. Only a slight influence of the ground simulation can be seen. The moving wall leads to somewhat higher pressures near the front of the car model. Because of thinner boundary layers and the kinetic energy brought in by the moving belt, a larger volume flow rate under the vehicle develops. Due to the continuity condition, a smaller volume flow rate with higher pressures above the vehicle then emerges.

In contrast, the underbody pressure reacts sensitively to parameter changes. Here, the boundary layers at the model and ground play an essential role. A moderate suction peak emerges at the curved lower underbody. Behind the peak, the flow is accelerated by increasing boundary layers and is then decelerated within the diffuser to the constant base-pressure. With increasing Re-numbers, the pressure drop under the model rises because the thickness of the boundary layers decreases and a larger volume flow rate with higher speeds under the car is apparent. The lift becomes more negative while the drag remains nearly constant for Re ≥ 7.0×10^5 (see Fig. 5).

The comparison of the moving to the stationary ground shows a larger negative lift ($c_{LP} = -0.88$) due to the kinetic energy given to the underbody flow by the moving belt and a smaller pressure drag ($c_{DP} = 0.32$) due to the non-separated diffuser flow. Figure 4 also shows that the pressure in the upper and lower separation point is nearly the same ($c_P = -0.33$). This pressure is imposed to the entire car base within the dead water. Hence, the base-pressure drag coefficients $c_{DP,B}$ of 0.27 and 0.26 respectively, totals between 75% and 81% of the entire pressure drag coefficient c_{DP} depending on the ground condition.

The aerodynamic model forces have been measured with the six-components-balance and the results are shown as function of u_∞ and Re in Fig. 5. Combined with the pressure measurements in Fig. 4 they indicate that the drag component due to friction to be nearly 20% of the total drag c_D, which is typical for such a two-dimensional bluff body near to the ground. At Re = 9.9×10^5 e.g., the drag in the case of the stationary ground is $c_D = 0.40$ ($c_{DP} = 0.36$) whereas for the moving ground it becomes $c_D = 0.39$ ($c_{DP} = 0.32$). The influence on the lift can be also seen. All pressure and force measurements show that statements about the behavior of motor vehicles in wind tunnels are only applicable when the ground is simulated correctly at high Re-numbers.

In Fig. 6, the consequences of the active flow control can be seen where the more interesting case of the moving ground is considered. If a volume flow rate of $V_{F,R} = 100$ l/s, $u_F = 20$ m/s and $u_R = 60$ m/s is taken from the ambient flow, is accelerated by an external periphery pump and then blown out across both rear slots, the shown pressure distributions with $c_{LP} = -0.66$, $c_{DP} = 0.33$ and $c_{DP,B} = 0.14$ appear. In the presented case, an additional splitter-plate of a standardized length of $l/L = 0.07$ (l: length of the plate) is attached to the base. Odenthal (1997) describes the influence of different

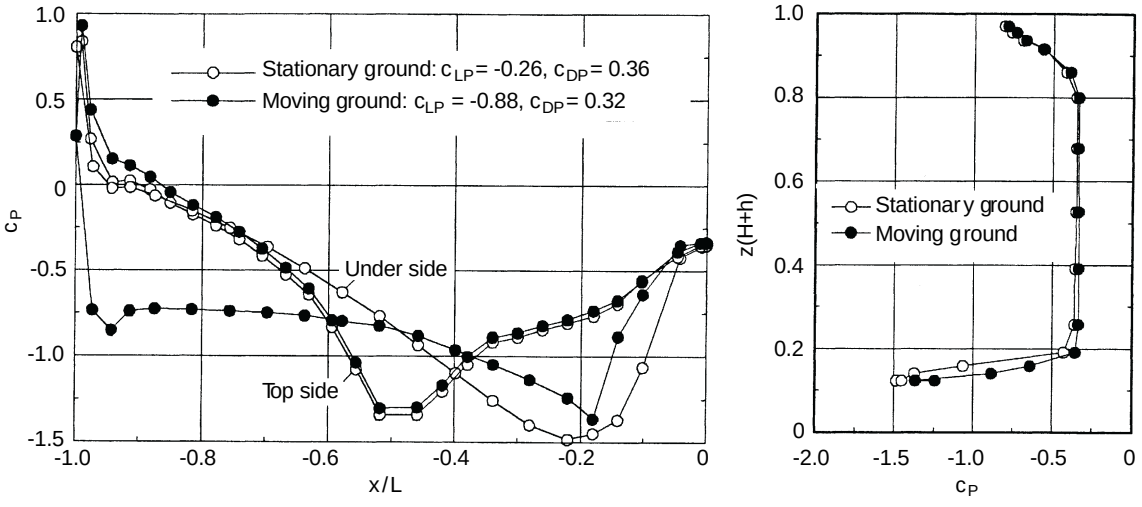

Fig. 4. Comparison of the pressure distributions in the middle span of the model for stationary and moving ground at Re = 9.9×10^5 and a ground clearance of $h/L = 0.04$

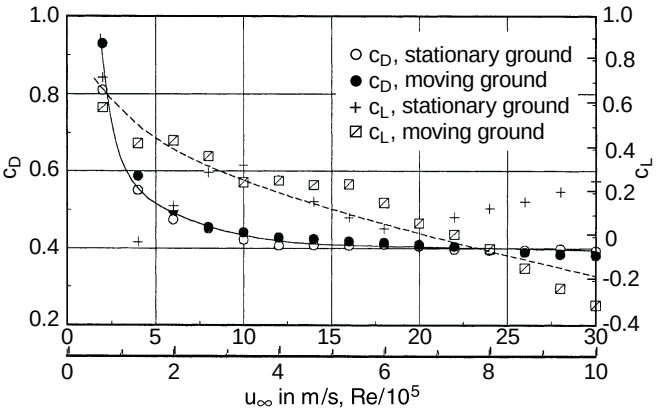

Fig. 5. Total lift and drag coefficients of the model determined from measurements with the six-components-balance at a ground clearance of $h/L = 0.04$ and a blowing rate of ζ_R=0

splitter-plates at the rear side of the current model. The chosen plate prevents best the direct clashing of the Coanda jets and therefore reduce dissipation effects as it is explained below.

It can be seen that the pressure drag has risen compared to the case without Coanda blowing. This first unexpected phenomenon has several explanations. On one hand, the pressure on the front surface increases due to the incoming stagnated air which causes momentum deficits. On the other hand, the ambient flow is entrained by the Coanda jets and is accelerated in the direction of the end of the model, whereby deeper pressures are projected on the contracted rear surface. Hence, the rise in pressure which is expected due to the avoided separation, is partially compensated and so additional forces in positive x-direction are induced. Likewise, suction peaks with pressure coefficients up to $c_P = -1.9$ close to the slots result from the flow control technique. It also has to be considered that the thrust of the jets working upstream is not contained in c_{DP} and $c_{DP,B}$. Furthermore, in Fig. 6 can be seen that both jets adheres to the curved base and this effect leads to a considerable rise in pressure of up to $c_P = 0.25$. In spite of the suction peaks the base-pressure drag coefficient is therefore reduced from $c_{DP,B} = 0.26$ to 0.14. This corresponds to a $c_{DP,B}$-reduction of nearly 50%.

Therefore, the new method seems to be more suitable for road vehicles without contracted tails, especially within the roof region. Thus, vertical projection areas with high suction peaks are avoided and the pressure drag is reduced. This design would be extremely effective e.g. for trucks. The systematic investigations in Odenthal (1997) have shown that the jet flow rate ζ_R may not be too high because of the above mentioned points, but should be in the region of $1.5 < \zeta_R < 2.5$.

However, no statements to the combined effect of rise of base-pressure and resulting thrust induced by the horizontal blowing components can be made. These effects can not be separated from one other and must be considered for a real motor vehicle, because both effects lead to drag reduction. Therefore, the investigations have been completed by measurements with the balance which registers both the rise of base pressure and the recoil of the Coanda jets.

Figure 7 compares the course of drag with and without flow control (see Fig. 5) as function of the Re-number Re and blowing rate ζ_R. In the presented investigations ζ_R could not be varied independently of Re since the velocity in the blowing slots was constant due to defect pump control. Nevertheless, the influence of the active flow control is recognized clearly. Although the integration along the base surface $h_B \times B$ leads to a slight rise of pressure due to the suction peaks, a negative drag is produced due to the thrust. With increasing Re-numbers the thrust decreases as the Coanda effect plays a more essential role. Considering all aerodynamic forces applied to the model, the total drag decreases by the Coanda-blowing, e.g. from $c_D = 0.39$ to $c_D = 0.35$ when $Re = 9.9 \times 10^5$. This benefits the drag up to 10%.

The investigations indicate that the base-pressure increases at moderately high blowing rates and that the total drag can be reduced. The following results of the LDA-measurements support these statements.

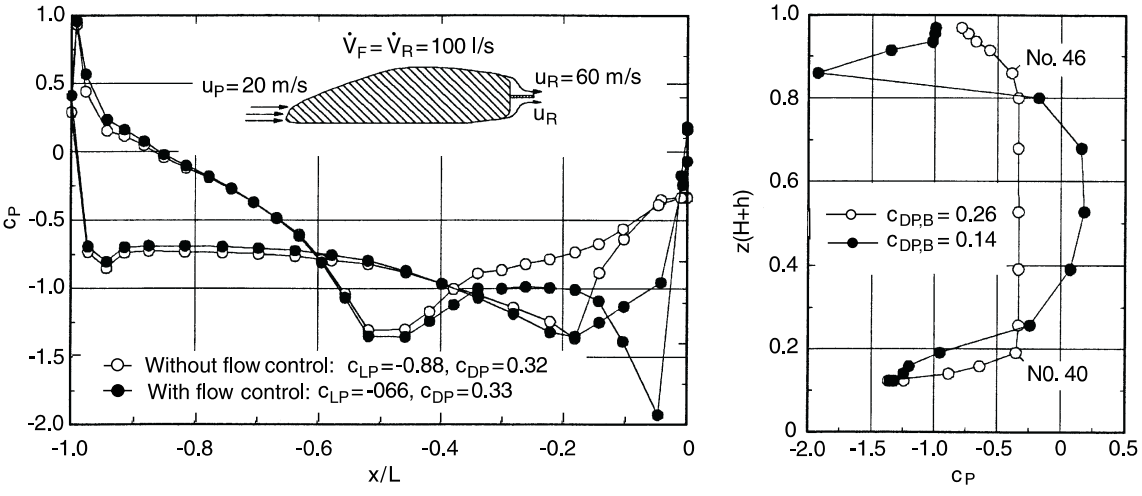

Fig. 6. Model pressure distributions at $Re = 9.9 \times 10^5$, moving ground and a ground clearance of $h/L = 0.04$; comparison without and with flow control (front suction and rear blowing, $\zeta_R = 2$)

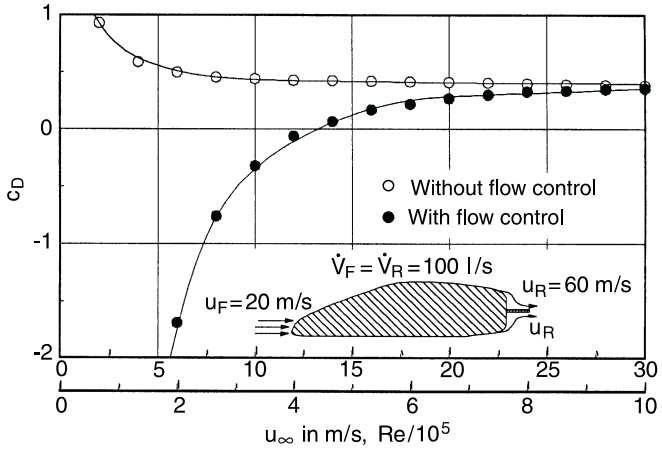

Fig. 7. Total drag coefficients determined from measurements with the six-components-balance at a ground clearance of $h/L = 0.04$

First, Fig. 8 shows the LDA-results in the dead water and far wake at Re = 6.6×10^5 with moving ground and $h/L = 0.04$. Unfortunately, no higher Re-numbers could be investigated because the tracer particles were then deposited at the walls of the wind tunnel. However, clear tendencies are already recognizable at Re = 6.6×10^5. The time averaged velocities have been standardized with the freestream velocity of $u_\infty = 20$ m/s which is presented in the left upper part of the diagram. All diagrams are based on LDA-measurements in three longitudinal model sections at $y/B = 0$ and ± 0.075. The three test series, each with 23×24 points were arithmetically averaged so that each figure is based on the values of 1656 points for 1000 samples per point. Additionally, the zero-streamline Ψ_0 enclosing the high turbulent dead water, is shown in Fig. 8a. The zero-streamline is defined as:

$$\Psi_0 = \frac{\Psi}{u_\infty L} = \frac{\int u(x,z)\mathrm{d}z}{u_\infty L} = -\frac{\int w(x,z)\mathrm{d}x}{u_\infty L} = 0 \ . \qquad (2)$$

In Fig. 8a can be seen that the outer flow accelerates up to 20% due to the displacement of the model. At the rear slots, the flow separates and two instable shear layers develop which interact in the back region of the dead water. The car model induces a converging flow with a distinctive recirculating zone and an asymmetric double vortex, which is characteristic for bluff bodies, as well as a momentum deficit in the wake. The maximum backflow velocity can be found between both vortex and totals approx. 30% of u_∞. The axial extension of the dead water is $x/L = 0.43$. The position of the free stagnation point is $x/L = 0.44$ and $z/(H + h) = 0.38$. The measurement of the pressures in this case leads to $c_{LP} = -0.54$, $c_{DP} = 0.33$ and $c_{DP,B} = 0.27$. The investigations in Odenthal (1997) show that the geometry of the dead water, the position of the stagnation point and the aerodynamic coefficients depend strongly on the Re-number, the ground clearance and the ground motion.

Figure 8b clearly shows, how the dead water is modified basically by the active flow control. Likewise, as shown in Fig. 6, a volume flow rate of $\dot{V}_{F,R} = 100$ l/s is taken with $u_F = 20$ m/s out of the forebody and is then blown out across the slots with $u_R = 60$ m/s. The data correspond to Re = 6.6×10^5 and $\zeta_R = 3$. Because of the somewhat slanted LDA-facility some points underneath the splitter plate could not be traversed. One can see that the Coanda jets quickly lose their kinetic energy due to turbulent mixing processes. The entrained flow is diverted and therefore separation is avoided. The jets run against the short splitter plate in the middle of the base. Because the division of the flow by the wedge to the upper and lower slot (see Fig. 3a) is not proportionate an easily downward slanted mixing jet emerges. Although the recirculating zone is completely eliminated and is replaced by free-stream fluid, the aerodynamic coefficients are still high ($c_{LP} = 0.51$, $c_{DP} = 0.50$, $c_{DP,B} = 0.31$). A reason for this could be that the main stream is put under considerably acceleration to the rear of the model, when the blowing rate is to high. Distinctive suction peaks simultaneously appear near the slots and the dissipation due to the clashing jets is high as well. When the Re-number is 6.6×10^5 e.g., the pressure coefficient within the upper slot (No. 40) is $c_P = -3.0$ and in the lower slot (No. 45) is $c_P = -1.8$. The pressure integration along the car model surface then causes a large pressure drag. However, punctual LDA-measurements at Re = 9.9×10^5 have shown that the main flow stay attached on the base in a similar way to the situation in Fig. 8b. In this case, the increasing base-pressure of up to 50% emerges because the suction peaks and dissipation effects get smaller.

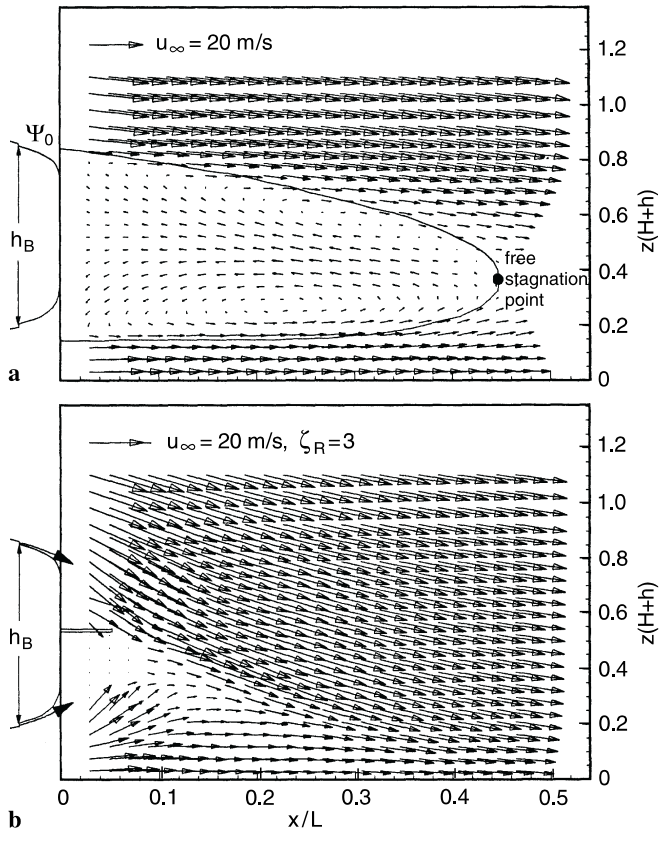

Fig. 8. Flow pattern (u,w) at Re = 6.6×10^5, moving ground, ground clearance $h/L = 0.04$; **a** without flow control, **b** with flow control ($\dot{V}_{F,R} = 100$ l/s) and splitter plate

As with the time averaged velocities of Figs. 8, 9 shows exemplary the turbulence energy k, defined as

$$k = \tfrac{1}{2}(\overline{u'^2} + \overline{w'^2}) \quad . \tag{3}$$

It is standardized with u_∞^2 and is a rate for the energy dissipation. When the dead water is not influenced (Fig. 9a), the turbulence energy rises along the free shear layers. The steep gradients of the velocity within the shear layers lead to a high Reynolds stress resulting in instability and rotation in the dead water. The maximum value of $k/u_\infty^2 = 0.065$ is obtained in the back region at $x/L = 0.45$ and $z/(H + h) = 0.40$. The comparison with Fig. 8a shows that these coordinates correspond to the position of the free stagnation point. Here, both shear layers interact and produce high turbulence energies due to the distinctive w'-components.

Blowing with $\zeta_R = 3$, as shown in Fig. 8b, avoids the recirculating zone with double vortex structure in the near wake, the time averaged velocity vectors are directed exceptionally downstream and have high values. In addition, according to Fig. 9b, the turbulence energy decreases considerably in the near wake. Indeed, the turbulence energy k is still high near the base of the car model and so the pressure drag is also high ($c_{D,P} = 0.50$). The last realization does not oppose the result shown in Fig. 7 that in the case of $\zeta_R = 3$ the total drag coefficient has the value $c_D = 0.28$. Since this value was determined by the balance, the total drag contains the thrust of the Coanda jets, too. But when the jet flow rate decreases to $\zeta_R \leq 2$, the kinetic energy of turbulence and the time averaged flow in the near wake is more and more transformed into pressure energy, where the raise in base-pressure and the drag reduction are found (see Figs. 6 and 7).

It is evident that the measurement of total lift and drag forces by a six-components-balance (see e.g. Englar et al. 1996) can not give unequivocal statements to the efficiency of the active flow control. Therefore, these facts will be clarified on the basis of momentum and energy consideration in the next section.

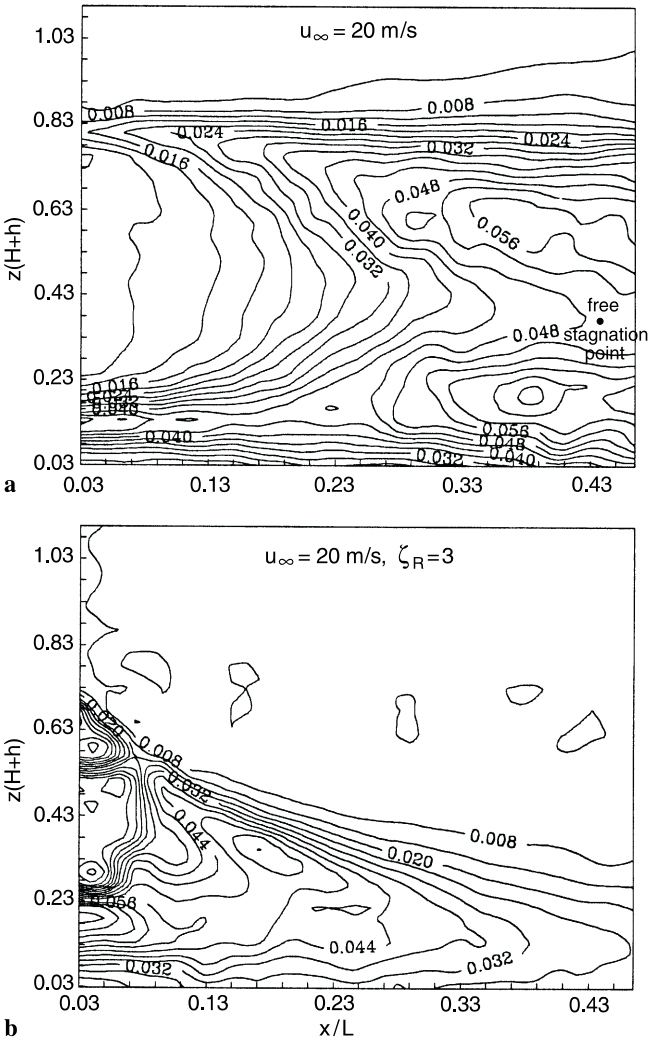

Fig. 9. Turbulence energy k/u_∞^2 at Re = 6.6×10^5, moving ground and a ground clearance of $h/L = 0.04$; **a** without flow control, **b** with flow control ($\dot{V}_{F,R}$=100 l/s) and splitter plate

4
Theoretical results

When air is taken from outside the test section of a wind tunnel by an external compressor and again is blown out of a model, mass, momentum and energy from outside the test section is given to the main stream. This process is not realistic because to simulate reality, the entire mass flow must be taken from the front of the model. An internal compressor should deliver the air to the rear, where it is blown out into the dead water. On the basis of mass, momentum and energy balance, some equations can be found determining the aerodynamic drag on the car model from the measured wake depression. These equations give information about, whether an energetic benefit of the described active flow control method exists or not. Naturally, the method will only be useful for a practical application if the compressor power for the active flow control is less than the engine power saved from drag reduction. As follows, the momentum and energy balances are applied to the two-dimensional model.

4.1
Momentum balance

The total drag F_D on a body essentially consists of the friction and pressure drag. The sum is called profile drag and can be determined by the momentum equation (e.g. Schlichting 1982). It states that the variation in momentum with time is equal to the external forces applied to the system. These outer forces are volume, pressure, friction and supporting forces. In the case of a stationary flow, the momentum equation is:

$$\begin{aligned}\frac{\mathrm{d}\overrightarrow{I}}{\mathrm{d}t} &= \sum \vec{F}; \int_{A_1} \rho \overrightarrow{v}(\overrightarrow{v}\,\vec{n})\mathrm{d}A \\ &= \overrightarrow{g}\int_V \rho\,\mathrm{d}V - \int_{A_1} p\vec{n}\,\mathrm{d}A + \int_{A_1} \overrightarrow{\tau}\,\mathrm{d}A \\ &\quad \underbrace{-\int_{A_2} p\overrightarrow{n}\,\mathrm{d}A + \int_{A_2} \overrightarrow{\tau}\,\mathrm{d}A}_{\vec{F}_S = -\vec{F}_D} \quad .\end{aligned} \tag{4}$$

The region A limiting the control surface is composed of a free surface A_1 and a body-fixed surface A_2 (see Fig. 10). The free surface A_1 is assumed to be far away from the body so that the friction produced by viscosity and turbulence – third term on the right side of Eq. (4) – can be neglected. In Eq. (4), the sum of the integrals along the surface A_2 is equal to the supporting force F_S acting in the opposite direction to F_D.

In both cases, with and without flow control, the drag F_D on a vehicle can be determined from the velocity profile in the wake, when an appropriate control region is chosen. In the non-influenced case, the control surface A_2 becomes equal to the surface of the car. But if the car is actively influenced, there will be difficulties due to several possible choices of the control surface. Firstly, it can be chosen so that the body-fixed surface A_2 increases up to the entire surfaces of the conduits. This means that within the model all aerodynamic forces induced by the inner flow will be a component of the supporting force F_S. The flow across the model remains unconsidered because it can be directly found as a momentum deficit in the wake. A second possibility to chose the control area will be discussed later.

The momentum equation is now applied to the ambient flow around the car model without flow control (subscript a) and with flow control (subscript b). In both cases the ground is moved. With stationary, frictional flow without gravity effects and using the definition of the total drag coefficient c_D,

$$c_{D,a,b} = \frac{F_{D,a,b}}{\frac{\rho}{2} u_\infty^2 BH} \quad , \tag{5}$$

in both cases we find:

$$c_{D,a,b} = \frac{2}{u_\infty^2 H} \int_0^\infty u_{34,a,b}\,(u_\infty - u_{34,a,b})\mathrm{d}z - \frac{F_{14,a,b}}{\frac{\rho}{2} u_\infty^2 BH} \quad . \tag{6}$$

The integral of the shearing stress along the free control surface A_1 must now be considered because of the no-slip-condition at the boundary A_{14}. Thus, Eq. (6) contains the friction force F_{14}, which is transmitted from the ground to the control surface A_{14}. Equation (6) can be applied to a car model with and without flow control.

To answer the question of the effectiveness of the method, the momentum balance in form of Eq. (6) can not be used. Obviously, an increasing blown out mass flow rate reduces the velocity deficit in the wake just as the drag calculated from Eq. (6). But it has to be considered that a larger compressor power must be available to transport the air across the model which may be larger than the power saved due to the drag reduction. It can be seen that a smaller velocity deficit in the wake does not automatically lead to a higher effectiveness of the method. Therefore, all mass flows passing the boundaries of the control surface may not be neglected, as shown in Fig. 10, but must be considered in the momentum balance.

To form the momentum equation with a modified control surface, the actively affected flow with moving ground will initially be discussed (subscript b). Thus, in Fig. 11 the chosen control area is shown. Applying the equation of continuity, we find:

$$\rho B \int_0^\infty u_{34,b}\,\mathrm{d}z + \rho B \int_0^I u_{23,b}\,\mathrm{d}x + \dot{m}_F - \dot{m}_{12} - \dot{m}_R = 0 \quad . \tag{7}$$

The left hand side of the momentum Eq. (4) in x-direction is:

$$\frac{\mathrm{d}I_{x,b}}{\mathrm{d}t} = \rho B \int_0^\infty u_{34,b}^2\,\mathrm{d}z + \rho B \int_0^I u_\infty u_{23,b}\,\mathrm{d}x + \dot{m}_F u_F - \dot{m}_{12} u_\infty - \dot{m}_R u_R \quad . \tag{8}$$

The right hand side of Eq. (4) is:

$$\sum F_{x,b} = p_\infty (A_{12} - A_{34}) + (p_R - p_\infty) A_R - (p_F - p_\infty) A_F - F_{12,b} - F_{D,b} \quad . \tag{9}$$

In all cases, the blown out air is completely taken from the front of the vehicle:

$$\dot{m}_F = \dot{m}_R = \dot{m} \quad . \tag{10}$$

Furthermore, the suction velocity can be expressed through the blowing velocity when the dimensions of the model slots are known:

$$u_F = u_R \frac{A_R}{A_F} \quad . \tag{11}$$

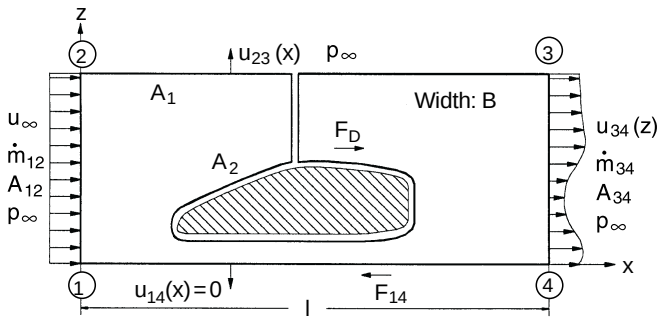

Fig. 10. To determine the drag of the model

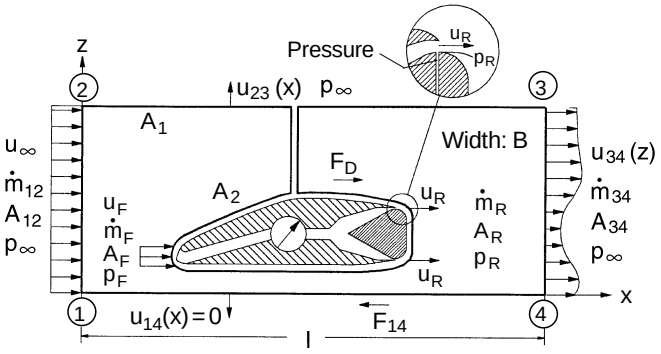

Fig. 11. Determination of the drag of the model with active flow control

The non-dimensional pressure coefficients are defined (see Fig. 11) as:

$$c_{P,F} = \frac{p_F - p_\infty}{\frac{\rho}{2} u_\infty^2} \quad \text{and} \quad c_{P,R} = \frac{p_R - p_\infty}{\frac{\rho}{2} u_\infty^2} \quad . \tag{12}$$

The flow can be seen to be dissipationless up to the front gaps. When the Bernoulli equation is applied to such a streamline and Eqs. (10), (11) and (12) are considered, the pressure coefficient within the front gaps is found to be:

$$c_{P,F} = 1 - \zeta_R^2 \left(\frac{A_R}{A_F}\right)^2 \quad . \tag{13}$$

Thus, the drag coefficient $c_{D,b}$ of the actively controlled model is:

$$\begin{aligned} c_{D,b} \;=\; & \frac{2}{u_\infty^2 H} \int_0^\infty u_{34,b}\,(u_\infty - u_{34,b})\mathrm{d}z \\ & + \left(2\,\zeta_R^2 \left(1 - \frac{A_R}{A_F}\right) + c_{P,R}\right) \frac{A_R}{BH} \\ & + \left(\zeta_R^2 \left(\frac{A_R}{A_F}\right)^2 - 1\right) \frac{A_F}{BH} - \frac{F_{14,b}}{\frac{\rho}{2} u_\infty^2 BH} \quad . \end{aligned} \tag{14}$$

Because the velocity distribution u_{34} in the wake includes all flow phenomena such as the Coanda effect and thrust, Eq. (14) considers all changes of the outer flow as well as the inner flow across the model. In order to check Eq. (14) by means of experimental results, the following simplifications must be made:

- The velocity distributions without and with flow control $u_{34,a}$ and $u_{34,b}$ can be measured at a large distance behind the model using the LDA. Likewise, the jet flow rate ζ_R can be determined exactly.
- The averaged pressure coefficient $c_{P,R}$ can be determined during the blowing out process because the pressure tabs No. 40 and 46 are positioned within the outlet of the slots.
- The friction force $F_{14,a,b}$ at the boundary A_{14} will be approximated by the skin-friction coefficient c_f on the laminar boundary layer along a flat plate (e.g. Schlichting 1982). This assumption must be made because the boundary layer distributions above the moving ground varied from the ideal rectangular contour. The value of $c_{F,a,b}$ in front of the vehicle is assumed to be zero.
- The ratio of the model surfaces are known to be $A_R/A_F = 0.3362$, $A_R/BH = 0.0170$, $A_F/BH = 0.0506$

These assumptions and Eq. (14) lead to:

$$\begin{aligned} c_{D,b} \;=\; & \frac{2}{u_\infty^2 H} \int_0^\infty u_{34,b}\,(u_\infty - u_{34,b})\mathrm{d}z \\ & + \frac{A_R}{BH} \left(\zeta_R^2 \left(2\frac{A_R}{A_F}\right) + c_{P,R}\right) \frac{A_F}{BH} - \frac{L}{H} \frac{1.328}{\sqrt{\mathrm{Re}}} \end{aligned} \tag{15}$$

Compared with Eq. (6), Eq. (15) is a further formula used to calculate the drag in the case of an active flow control. Only the second and third term on the right hand side of Eq. (15) differ which can be taken as a thrust component. While Eq. (6) considers an additional thrust as a decrease in drag – as it is usual for real vehicles – the above mentioned terms are now separated from the wake deficit. This means that the drag increases when the jet flow rate increases. It is therefore possible to make assumptions about the power benefit as shown in Fig. 12.

4.2 Energy balance

Because the momentum balances (6) and (15) require the knowledge of the velocity distributions in the wake, the power benefit of a motor vehicle can also be calculated from the energy equation. It must be assumed that the constant aerodynamic engine power P is available. The engine power consists of the part required to overcome the aerodynamic drag, but not the power due to the mechanical friction which is transferred to the wheels. To influence the dead water by blowing, the compressor power P_C must increased furthermore. Because P_C should be taken directly from the vehicle engine and thus has to be seen as a component of the aerodynamic engine power, only an approximate P_C reduced power is available to overcome the drag F_D. The energy balance is therefore:

$$F_D u_\infty = P - P_C \quad . \tag{16}$$

The aerodynamic drag F_D on the vehicle contains all flow phenomena (e.g. Coanda effect, thrust and inner flow effects). The compressor power is defined as:

$$P_C = \eta_C \,\Delta p_C \dot{V} = \eta_C \,\Delta p_C \,u_R \,A_R \quad . \tag{17}$$

Here, η_C is a loss factor which considers all pressure drops appearing in reality in the inlet and outlet pipes of the compressor as well as its efficiency, Δp_C is the produced increase of pressure of the pump which can be determined from the dissipative Bernoulli equation:

$$\Delta p_C = \frac{\rho}{2} u_\infty^2 (\zeta_R^2 + c_{P,R} - 1) \quad . \tag{18}$$

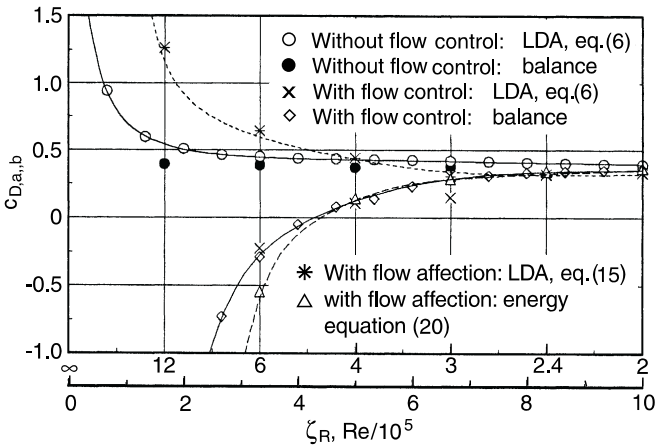

Fig. 12. Drag coefficient $c_{D,a,b}$ without (**a**) and with (**b**) active flow control ($\dot{V}_{F,R}$=100 l/s, u_F=20 m/s, u_R=60 m/s), moving ground, h/L = 0.04

Using definition (5) and inserting Eqs. (17) and (18) into the energy Eq. (16), we find that:

$$c_D = \frac{P}{\frac{\rho}{2} u_\infty^3 BH} - \eta_C \zeta_R \frac{A_R}{BH} (\zeta_R^2 + c_{P,R} - 1) \quad . \tag{19}$$

At the given aerodynamic engine power P, the freestream velocity u_∞ as well as the geometric factors A_R and the projected surface BH, the drag coefficient c_D of the influenced vehicle can be found as a function of η_C, ζ_R and $c_{P,R}$.

Conferring Eq. (19) on the current model, it can be seen that the first term on the right hand side corresponds to the drag coefficient $c_{D,a}$ without flow control (subscript a) because the second term becomes zero when ζ_R is zero. At the same engine power and the same main speed, the drag coefficient with active flow control is therefore (subscript b):

$$c_{D,b} = c_{D,a} - \eta_C \zeta_R \frac{A_R}{BH} (\zeta_R^2 + c_{P,R} - 1) \quad . \tag{20}$$

The derived Eqs. (6), (15) and (20) give an answer to the drag coefficient of the car.

To examine the derived equations by use of experimental results, LDA-measurements in the wake of the model were carried out at $x/L = 1.1$. There, the static pressure is almost exactly equal to the pressure of the undisturbed stream. At known velocity distributions $u_{34,a}$ and $u_{34,b}$ for the model without and with active flow control, the drag coefficients can be determined from the Eqs. (6), (15) and (20). All investigations in Fig. 12 show that the wake depression continually decreases with increasing jet flow rates ζ_R. When ζ_R becomes larger than four, no more depression can be found and a clear excess of kinetic energy develops.

Figure 12 shows the drag coefficient $c_{D,a,b}$ of the car model plotted as a function of Re-number and jet flow rate ζ_R. The results of the balance measurements and the LDA-measurements are compared. In general, it can be seen that a very good accordance between both principles of measurement exists. If the drag is calculated from the momentum Eq. (6), slight differences appear at small Re-numbers because the balance measurements are inaccurate due to small aerodynamic forces. In the case of the car model with an actively influenced flow, larger forces are transmitted to the balance and the differences between both principles become minimal. A clear and expected reduction in $c_{D,b}$ is seen in the graph. With increasing Re-number, that is to say with decreasing jet flow rate ζ_R, the drag rises because of the decreasing thrust. The Coanda effect still occurs and an irrotational dead water with higher base-pressures is induced for approx. $\zeta_R < 3$. The drag coefficient e.g., drops from 0.39 to 0.35 at $Re = 9.9 \times 10^5$ ($\Delta c_D = 10\%$).

When the drag is determined from the modified momentum Eq. (15), a large positive drag develops at small Re-numbers and high blowing rates, respectively. The reason for this effect is that the thrust is now considered separately from the wake depression and therefore is interpreted as a rise in drag. At $\zeta_R < 4$, the drag drops below the value of the non-influenced vehicle for the first time, resulting in a power benefit. It can be assumed that in the region of $1.5 < \zeta_R < 2.5$, the drag reduction compared to the compressor power has an optimal value as only then does a high base-pressure and low turbulence energy in the wake appear. In this case, the drag decreases even from 0.39 to 0.33 at a given Re-number of 9.9×10^5 (drag reduction 15%).

The c_D-course, calculated from the energy Eq. (20), is presented likewise. Considering the losses within the test facility as well as the efficiency of the pump with an estimated loss factor of $\eta_C = 0.3$ and taking the measured values of ζ_R, $c_{P,R}$ and $c_{D,a}$ as a basis, one obtains the results as shown in the graph. It can be seen that $c_{D,b}$ becomes positive for approx. $\zeta_R = 4.5$, so that the useful power becomes larger than the used power due to the blowing. Indeed, this statement is to be understood as an approximation because the loss factor had to be estimated. However, this factor can be clearly determined from the measured loss of pressure from a real motor vehicle.

With regard to the active flow control technique, the following conclusions can be made: A high blowing rate of $\zeta_R > 6$ produces a large propulsion of the car model due to the exhaust momentum. As the pressure graphs have shown, two considerable suction peaks appear at the base decreasing the rise in total base-pressure. A dead water with high kinetic turbulence energy then develops. Moreover, the entrained ambient flow is accelerated to the rear of the model and therefore additional force components in the direction of the drag emerge. In this case, the negative drag (see Fig. 12) is mainly attributed to the thrust of both jets. This effect is not desirable from an energetic point of view.

If the jet flow rate ζ_R decreases, the drag of the non-influenced and influenced model will converge. Using the momentum Eq. (15), it can be seen that for approx. $\zeta_R < 3.5$, a power benefit exists. The energy Eq. (20) with $\zeta_R < 4.8$ gives a higher value because the loss factor η_C could be only estimated. However, in contrast to the momentum equation, it does not need a statement about the velocity distributions in the wake.

$1.5 < \zeta_R < 2.5$ gives the best results. All measurements show that for $\zeta_R \approx 2$, the base-pressure coefficient $c_{DP,B}$ can be reduced by about 50%. Simultaneously, the total drag of the model reduces by about 10%.

5 Conclusions

The present investigation of a 1/5th scale two-dimensional car shaped body in a wind tunnel with moving belt simulation shows that lift and drag depend strongly on the Re-number and the conditions of the ground. Thus, the simulation of the relative motion between model and ground and realization of high Re-numbers is very important for correct statements about the aerodynamic coefficients. The results of active flow control techniques according to Geropp (1991, 1995) indicate that it is possible to reduce the drag. Therefore, a part of the main flow must be taken from the front of the model. The flow is accelerated within the model and then is tangentially blown out into the dead water. The jets stay attached on the base of the model due to the Coanda effect. They en-

train the ambient flow and cause a rise of base pressure. When the blowing rate is equal to two, the base pressure rises by nearly 50% while the total drag decreases by 10%. Measurements with a LDA show that a proportionate loss vortex dead water develops with decreasing blowing rates and that the turbulence energy in the wake decreases to a value below that of the non-influenced model. A power benefit can be clearly observed for moderately high blowing rates by using the momentum and energy equation. With regard to a real passenger car, this means that the compressor power used for the blowing technique could be taken from the vehicle engine but simultaneously the aerodynamic drag can still be reduced. Further investigations on a three-dimensional car model or a real motor vehicle should be carried out to elucidate the physical effects and the effectiveness of the method more effectively.

References

Apelt CJ; West GS; Szewczyk A (1973) The effects of wake splitter plates on the flow past a circular cylinder in the range $10^4 < \mathrm{Re} < 5 \times 10^4$. J Fluid Mech 61: 187–198

Bearman PW; De Beer D; Hamidy E; Harvey JK (1988) The effect of a moving floor on wind tunnel simulation of road vehicles. SAE-Paper 880245

Eberz T (1997) Dreidimensionale Turbulenz- und Wirbelstrukturen im abgelösten Gebiet eines Fahrzeugmodells. In: Turbulenz in der Strömungstechnik (Hrsg. Kim, M.S.), Shaker Verlag: 34–46

Englar RJ; Smith MJ; Niebur CS; Gregory SD (1996) Development of Pneumatic Aerodynamic Concepts for Control of Lift, Drag and Moments plus Lateral/Directional Stability of Automotive Vehicles. SAE Paper 960673: 27–38

Fernholz H-H (1966) Zur Umlenkung von Freistrahlen an konvex gekrümmten Wänden (Coanda-Effekt). DLR-Fachbericht 66–21

Freund JB; Mungal MG (1994) Drag and wake modification of axisymmetric bluff bodies using Coanda blowing. J Aircraft Vol. 31, No 3, 572–578

Geropp D (1991) Reduktion des Strömungswiderstandes von Fahrzeugen durch aktive Strömungsbeeinflussung. Patentschrift DE 3837729

Geropp D (1995) Process and device for reducing the drag in the rear region of a vehicle, for example, a road or rail vehicle or the like. U.S. Patent 5,407,245

Geropp D; Kim MS (1995) Zonenmethode zur Berechnung ebener Körperumströmungen mit Totwasser und Bodeneinfluß. Arch Appl Mech 65: 270–278

Geropp D; Mildebrath T (1995) Berechnung dreidimensionaler abgelöster Strömungen mit Bodeneinfluß. DGLR-Jahrbuch 1995: 895–904

Gersten K; Wiedemann J (1982) Widerstandsverminderung umströmter Körper durch kombiniertes Ausblasen und Absaugen an der Wand. Forschungsbericht des Landes NRW 3103, Fachgruppe Maschinenbau/Verfahrenstechnik, Westdeutscher Verlag

Han T; Sumantran V; Harris H; Kuzmanov T; Huebler M; Zak T (1996) Flow-Field Simulation of Three Simplified Vehicle Shapes and Comparison with Experimental Measurements. SAE Paper 960678: 75–90

Hucho WH (1994) Aerodynamik des Automobils. VDI-Verlag, 3. Auflage

Kronast M (1992) Einfluß eines ruhenden und bewegten Bodens auf die Umströmung zwei- und dreidimensionaler Fahrzeugmodelle. VDI-Reihe 7–205

Leder A (1992) Abgelöste Strömungen-Physikalische Grundlagen. Vieweg Verlag, 1. Auflage

Odenthal H-J (1997) Kfz-Totwasserströmungen mit Fahrbahnwechselwirkung und aktiver Strömungsbeeinflussung zur Widerstandsreduktion. VDI-Reihe 7–307

Ramnefors M; Bensryd R; Holmberg E; Perzon S (1996) Accuracy of Drag Predictions on Cars Using CFD – Effect of Grid Refinement and Turbulence Models. SAE Paper 960681: 121–135

Schlichting H (1982) Grenzschichttheorie. G. Braun Verlag, 8. Auflage

Soja H (1994) Beeinflussung des Hecktotwassers an Fahrzeugkörpern in Bodennähe und dessen Auswirkung auf die aerodynamischen Beiwerte. Dissertation, Universität Stuttgart

Truckenbrodt E (1980) Fluidmechanik. Springer Verlag, 2. Auflage

Wiedemann J (1989) Some basic investigations into the principles of ground simulation techniques in automotive wind tunnels, SAE-Paper 890369